Visualization of Density Variation in Lung Nodules

Aristófanes C. Silva
e-mail: ari@inf.puc-rio.br

Paulo Cezar P. Carvalho
Instituto de Matemática Pura e Aplicada - IMPA
Estrada D. Castorina, 110, 22460-320, Rio de Janeiro-RJ
e-mail: pcezar@impa.br

Marcelo Gattass
e-mail : gattass@tecgraf.puc-rio.br

Abstract

We propose a method for visualize lung nodule, in order to emphasize their internal structures. This provides an additional tool for diagnosis, which is traditionally based on the analysis of shape, growth and location. The method is divided into three stages: the first stage is semi-automatic segmentation, using the region-growing algorithm; the second stage, based on the previous segmentation, identifies the internal structures of the nodule using moment theory to determine several thresholds; finally, in the third stage, to help visualizing these structures, a pseudocolor is associated to each threshold determined in the previous stage. The tool developed is under tests, undergoing clinical evaluation, and its initial results are promising.

Keyword : visualization, segmentation, region growing, moment, histogram, threshold.

Resumo

O método proposto neste trabalho visualiza as estruturas do nódulo pulmonar de modo a enfatizá-las, o que possibilita uma forma adicional de diagnóstico, além das tradicionais baseadas em forma,

crescimento e localização. O método está dividido em três fases. A primeira fase a segmentação semi-automática, utilizando o algoritmo de região de crescimento. A segunda fase, baseada na segmentação anterior, identifica as estruturas internas do nódulo usando a teoria de momentos para determinar vrios limiares. Por fim, na terceira fase, para facilitar a visualização destas estruturas, é associada uma pseudocor a cada limiar determinado na fase anterior.

A ferramenta desenvolvida está em fase experimental e encontra-se sob avaliação clínica, sendo os resultados iniciais promissores.

Palavras-chave : visualização, segmentação, região de crescimento, momentos, histograma, limiar.

1 Introduction

Lung cancer is known to be the form of cancer with the smallest survival rate after the diagnosis, with a gradual increase in the number of deaths every year (Tozaki et al., 1996). For this reason, the sooner it is detected, the greater the possibility of cure. On the other hand, the more information the doctor has available, the more precise is the diagnosis.

Images acquired through computer tomography (CT) allow the identification of lung structures both normal and pathologic, such as nodules, but cannot show in detail their internal structures. Such structures (calcification, fibrosis, necrosis, fat, etc.) provide the doctors important data for a more precise diagnosis. For instance, the existence and location of calcifications, regions with necrosis and fat can suggest the nodule's benignity of malignity (Jain, 2001). However, the visualization of such structures can be very difficult, or even impossible, for the human eye.

Several works were developed with the purpose of diagnosing lung nodules with computer assistance, but they focus on analyzing their shape (Tozaki et al., 1996; Kanazawa et al., 1998; Fan et al., 2001; Reeves and Kostis, 2000; Erberich et al., 1999) (circular, spiculated, etc.); growth (Fan et al., 2001; Reeves and Kostis, 2000; Ko and Betke, 2001; Yankelevitz et al., 2000), based on their diameter or volume; or location (Kanazawa et al., 1998; Reeves and Kostis, 2000), either central or adjacent to the pleura. In the present work, a new form of computer-aided analysis and diagnosis of lung nodules will be proposed, with emphasis on the identification and visualization of the nodule's internal structures. This method has been successfully used in the segmentation and identification of breast lesions (Anguh and Silva, 1997). It was observed that the difficulties in identifying breast lesions are similar to those for lung nodules, since both have calcifications of varied shapes and sizes, and structures with high and low densities. This causes the internal structures and tissues to mix in the visualization, causing difficulties.

The tool developed can be applied to high-dose, multislice or low-dose (for screening) CT. It runs on several platforms and uses a simple PC, which makes it cheap and accessible to small companies and individual doctors.

The proposed method is divided into three stages. The first stage is

1

semi-automatic segmentation, using the region-growing algorithm, with the purpose of extracting the region of interest - the nodule. The second stage, based on the previous segmentation, identifies the internal structures of the nodule using moment theory to determine several thresholds. Finally, in the third stage, to help visualizing the detected structures, a pseudocolor is attributed to each threshold determined. Also, in this stage, the histogram of such structures is computed, so that the doctors know how many voxels they contain. The results of the tests performed by specialized doctors and the preliminary evaluation are very encouraging.

This article is organized as follows: Section 2 provides the mathematical basis of the moment theory for automatic threshold determination and describes each stage of the method; Section 3 analyzes the method's application; finally, Section 4 analyzes the results obtained.

2 The Method

2.1 Mathematical Basis of the Method

This section provides mathematical support to understand the proposed method, describing each stage.

2.1.1 Moments

Let us consider a 3D image with intensities given by $i = f(j, k, l)$, where $0 \leq j \leq J - 1$, $0 \leq k \leq K - 1$ and $0 \leq l \leq L - 1$. Its rth moment will be defined by:

$$M_r = \frac{1}{N} \sum_{j=0}^{J-1} \sum_{k=0}^{K-1} \sum_{l=0}^{L-1} f(j, k, l)^r \tag{1}$$

Moments can also be defined in terms of the image histogram and are

2

given by:

$$M_r = \frac{1}{N} \sum_{i=0}^{P-1} h(i)i^r \qquad (2)$$

where $h(i)$ is the ith value in the histogram, P represents the densities, and N is the total number of voxels in the nodule.

The mean of the distribution, $m = M_1$, is used to compute the rth central moment, defined as:

$$M_r = \frac{1}{N} \sum_{j=0}^{J-1} \sum_{k=0}^{K-1} \sum_{l=0}^{L-1} (f(j,k,l) - m)^r \qquad (3)$$

The central moment using the histogram is given by:

$$M_r = \frac{1}{N} \sum_{i=0}^{P-1} h(i)(i - m)^r \qquad (4)$$

Central moments M_2 - the variance, which provides contrast information - and M_3 - which provides symmetry information - are especially important.

More detailed information on moment theory can be found in (Castleman, 1996; Gonzalez and Woods, 1992; Jain, 1989).

2.1.2 Threshold

An image with a bimodal histogram allows an easy determination of a threshold for segmentation. However, bimodal images are rare. To determine an optimum threshold to segment an image which is not bimodal, one must reduce segmentation error to the minimum. (Wood and Jamali, 1992) used a cost function, which is the sum of the product of the distance to the square of each two-mode voxel value, a and b, to minimize threshold error. This function is given by:

$$e = \sum_{j=0}^{J-1} \sum_{k=0}^{K-1} \sum_{l=0}^{L-1} (f(j,k,l) - a)^2 (f(j,k,l) - b)^2 \tag{5}$$

Minimizing the cost e in Equation 5, we have:

$$a = \frac{c_1 - \sqrt{c_1^2 - 4c_2}}{2} \tag{6}$$

$$b = \frac{c_1 + \sqrt{c_1^2 - 4c_2}}{2} \tag{7}$$

where

$$c_1 = \frac{M_3 - M_1 M_2}{M_2 - M_1^2} \tag{8}$$

$$c_2 = \frac{M_1 M_3 - M_2^2}{M_2 - M_1^2} \tag{9}$$

The threshold value will be given by:

$$T = \frac{(a+b)}{2} \tag{10}$$

If the nodule's intensity is constant, then $f(j,k,l) = m$ and $M_r = 0$, for $r \geq 1$. Also, if $(a+b) = 0$, c_1 and c_2 will be zero, therefore the value that minimizes the error will be m.

2.2 Description of the Method

2.2.1 Region Growing

The first stage of the method consists in determining, with specialist support, where the nodule of interest is located. For such, we used the region-growing algorithm with voxel aggregation in 3D (Castleman, 1996; Gonzalez and Woods, 1992; Jain, 1989; Nikolaidis and Pitas, 2001), as it allows great

interaction with the medical doctors. Apart from this algorithm, two tools were implemented that support and allow greater control over the segmentation: barrier and eraser. The barrier is a cylinder around the nodule which limits the region of interest and prevents the segmentation from invading lung structures other than the nodule. The eraser allows the doctors to erase unwanted structures near the nodule, either before or after segmentation, to prevent and correct possible errors.

2.2.2 Thresholds

The mathematical basis described in Section 2.1 is used to automatically generate thresholds with values $T_n, n = 0, ..., P - 1$, to detect nodule structures (Anguh and Silva, 1997). The histogram, its equalization and its moments are employed to determine such thresholds: the nodule's histogram provides information on density distribution, the equalization is used to enhance the nodule's quality, and the moments (mean, variance and symmetry) show how the nodule's densities vary and their tendency in relation to the average.

The equalization is applied to the original nodule and, by means of the histogram, the moments are computed (Equations 2 and 4) to determine the first threshold, T_1 (Equation 10). This process is repeated to determine the following thresholds (T_n), but considering only voxels in the volume having density larger than the previous threshold T_{n-1}.

The threshold generation process ends considering the following convergence criteria:

- $T_n > P - 1$. The threshold value is greater than the maximum number of thresholds, a value specified by the user.

In practice, it is more useful to apply the above method considering only the voxels whose densities exceed a given value. This discards uninteresting, low-density regions of the volume, focusing on the high-density regions associated with the occurrence of nodules, calcifications, fibrosis, etc. The method can be easily adapted to accomodate this modification. It suffices

to specify a initial threshold value T_0. We have found that using the mean density m provides good results.

2.2.3 Pseudocolor

The human visual system is able do discern only a limited number of gray tones, so the visualization of all thresholds together, representing the nodule's structures, becomes confusing. Therefore, a specific pseudocolor was associated to each threshold, coloring the nodule to help visualization.

Considering different thresholds with value T_n and different colors C_n, for $n = 0, ..., N-1$, where $N \leq P$, the pseudocolor mapping will be described by $f(j,k,l) = C_n$, where $T_n \leq f(j,k,l) < T_{n+1}$, where $f(j,k,l)$ is the original density of the nodule's voxel. In this work, to make visualization easier, the pseudocolors were defined in hues of red. The greatest intensity was associated to the highest threshold, and the smallest intensity was associated to the lowest threshold, as illustrated in Fig. 1. There is no relationship between the selected colors and the specific structures.

Fig. 1: Pseudocolor palette.

2.3 Algorithm

```
Segment nodule with region growing
Detect thresholds for nodule
  compute histogram h[i],  i = 0, ..., P − 1  de  f(j, k, l)
  while  true
  {
      equalize histogram in interval T_{n−1} to T_{n+1}
      compute natural moment,  m = M_1
      compute central moment,   M_2 e M_3
```

6

```
        compute a and b
        if  termination condition then
              break
        else
          Tₙ  =  0.5(a  +  b)
    }
    Attribute pseudocolor f(j,k,l)  =  Cₙ, where  Tₙ  ≤  f(j,k,l)  <  Tₙ₊₁
```

$$\text{compute } a \text{ and } b$$
$$\text{if } \textit{termination condition} \text{ then}$$
$$\quad \text{break}$$
$$\text{else}$$
$$T_n = 0.5(a + b)$$
$$\}$$
$$\text{Attribute pseudocolor } f(j,k,l) = C_n, \text{ where } T_n \leq f(j,k,l) < T_{n+1}$$

3   Discussion

In this section, we will analyze the application of the algorithm to CT slices. The case is that of a patient in whom a nodule with central calcification was detected and diagnosed as benign. 33 slices of the nodule were evaluated. Fig. 2 shows a slice in which the calcification is in evidence. One can see, however, that using the lung window (1500 HU [Hounsfield Unit]/−700 HU) it is impossible for the doctors to visualize areas with different densities inside the nodule. On the other hand, using the mediastinum window (350 HU/40 HU), it was possible to identify an area of rough calcification, according to its irregular density (Fig. 3). However, even in the mediastinum window, it is difficult to discern subtle variations in the composition. The proposed method seeks to improve this deficiency.
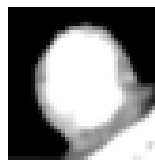

Fig. 2: Nodule - lung window.

Fig. 3: Nodule - mediastinum window.

The nodule in Fig. 3 was segmented with the region-growing algorithm, with initial threshold of −450 HU and final threshold of 1200 HU. Then, thresholds were determined to detect the nodule's structures. Fig. 4 to 11 show the application of each threshold to the nodule, and Fig. 12 displays the application of all thresholds. Eight thresholds were determined, with HU

values 602, 1205, 1536, 1717, 1824, 1907, 1958 and 1986. Finally, a pseudocolor was attributed to each threshold.

Fig. 4: T≤ 602.

Fig. 5: 602 ≤T< 1205.

Fig. 6: 1205 ≤T< 1536.

Fig. 7: 1536 ≤T< 1717.

Fig. 8: 1717 ≤T< 1824.
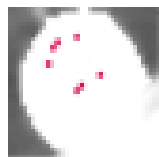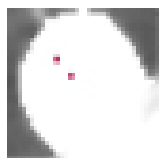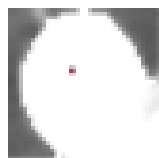

Fig. 9: 1824 ≤T< 1907.

Fig. 10: 1907 ≤T< 1958.

Fig. 11: 1958 ≤T< 1986.

Fig. 12: Final image.

The nodule in Fig. 12 has a volume of 6214 voxels, and Fig. 13 shows its histogram after the structures were detected. With such information, the doctors can evaluate how many voxels each structure has, which can provide them a dimension of its size and proportion in relation to other nodule structures.

According to the tests performed, we observed that, from the sixth threshold on, there is no significant visual change in the image. Therefore, in most cases, six thresholds will be enough.
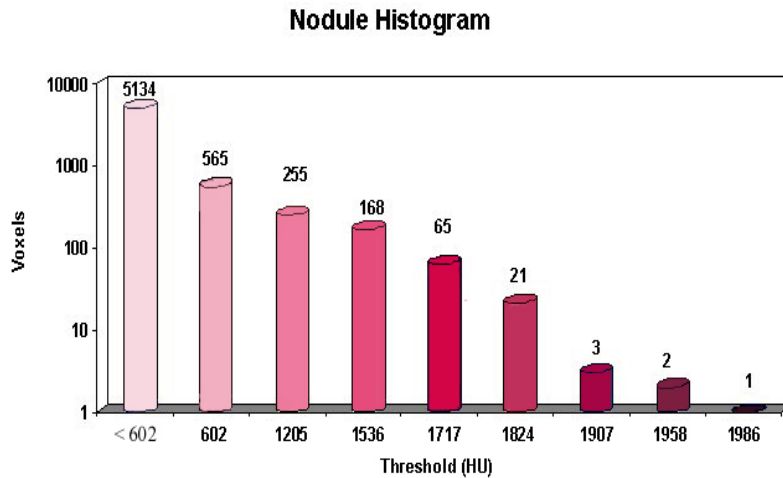
Fig. 13: Histogram of the identified structures.

The images were acquired with a Helicoidal GE pro Speed tomograph under the following conditions: pipe voltage 120 Kv, pipe current 100 mA, image size 512x512 pixels, and reconstruction interval 2 mm. The images were quantized in 12 bits and stored under the DICOM format.

The software was implemented in C++, using two additional libraries developed by the Tecgraf computer graphics laboratory, IUP (Levy et al., 1996) and CD (TecGraf, 2001), for interface and drawing, respectively, and was compiled with Microsoft's Visual C++. The platform necessary for the tool's execution is a PC with Unix, Linux or Windows operating system.

4   Results

The tests were performed with exams from 30 patients with several pathologies. To demonstrate the results obtained, two cases with different levels of complexity will be shown.

1. Patient A

In the preliminary diagnosis, the doctors detected a homogeneous low-density nodule. Fig. 14 shows the region of the CT slice where the nodule was found in the mediastinum window.

Fig. 15 presents the result of the method's application. Two regions of interest inside the nodule were detected, one with high density and the other with low density. The low-density region (-53 HU) is indicated with the arrow to the right and is possibly a necrosis area. The high-density region (> 103 HU), indicated with the arrow to the left, is possibly a calcified area. The patient was operated, and the histopathological diagnosis was tuberculoma, with areas of caseosa necrosis detected.
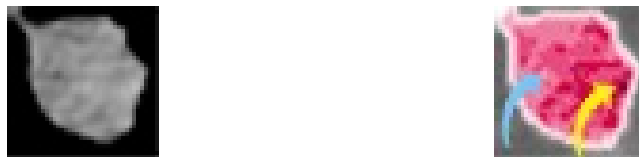

Fig. 14: CT slice with the nodule from Patient A.

Fig. 15: Structures detected in the nodule from Patient A.

2. Patient B
   In the preliminary diagnosis, a visually homogeneous nodule was detected, with areas of low and high densities and a large calcified area in the inferior boundary of the nodule. Fig. 16 shows the region of the CT slice of the module in the mediastinum window.

   After applying the method to the module, a large region was detected, in the right inferior section of the nodule, with higher density. Fig. 17 presents the method applied to the nodule; the calcified region (> 224 HU) is indicated by the arrow. At the time of writing, a final diagonosis was not available for this pacient, but doctors suspect the nodule to be malignant, especially due to the location of the lesion.

5   Conclusion

The proposed method detects structures in lung nodules, allowing an alternative form of diagnosis apart from the traditional ones, based on shape, growth
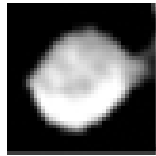
Fig. 16: CT slice with the nodule Fig. 17: Structures detected in the
from Patient B.   nodule from Patient B.

and location. The method is composed of three stages: nodule segmentation,
using the region-growing algorithm; automatic detection of nodule structures,
using several thresholds; and association of pseudocolors to the thresholds.

The visualization of nodule structures with colors helps identifying high-
or low-density areas, which can be associated, for instance, with calcifications
or areas of necrosis, even though the colors' purpose is only to allow a better
visualization of the nodule. The results obtained allow better visualization
of the internal structures of the nodule.

The method presented is undergoing tests and clinical evaluation. Its
initial results are promising.

Acknowledgments

References

Anguh, M. M., Silva, A. C., 1997. Multislice segmentation and enhancement
in mammograms. In: X Simpósio Brasileiro de Computação Gráfica e Pro-
cessamento de Imagem. IEEE Transactions on Computers, pp. 136–139.

Castleman, K. R., 1996. Digital Image Processing. Prentice Hall, Englewood Cliffs, NJ, USA.

Erberich, S. G., Song, K.-S., Arakawa, H., Huang, H. K., Webb, R., Hoo, K. S., Loo, B. W., 1999. Knowledge-based lung nodule detection from helical CT. Bildverarbeitung für die Medizin , 337–341.

Fan, L., Novak, C. L., Qian, J., Kohl, G., Naidich, D. P., 2001. Automatic detection of lung nodules from multi-slice low-dose CT images. In: SPIE Medical Imaging. San Diego, CA.

Gonzalez, R. C., Woods, R. E., 1992. Digital Image Processing, 3rd Edition. Addison-Wesley, Reading, MA, USA.

Jain, A. K., 1989. Fundamentals of Digital Image Processing. Prentice Hall, Englewood Cliffs, NJ, USA.

Jain, D., 2001. Understanding the solitary pulmonary nodule, available at: [http://indegene.com/Pul/FeatArt/indPulFeatArt3.html]. Accessed November 21, 2001.

Kanazawa, K., Kawata, Y., Niki, N., Satoh, H., Ohmatsu, H., Kakinuma, R., Kaneko, M., Moriyma, N., Eguchi, K., 1998. Computer-aided diagnosis for pulmonary nodules based on helical CT images. Computered Medical Imaging and Graphics 22, 157–167.

Ko, J. P., Betke, M., 2001. Chest CT : Automated nodule detection and assessment of change over time - preliminary experience. Radiologic Clinics of North America 218, 267–273.

Levy, C. H., Figueiredo, L. H., Gattass, M., Lucena, C. J. P., Cowan, D., 1996. IUP : A portable user interface development tool. Software : Practice and Experience 267, 737–762.

Nikolaidis, N., Pitas, I., 2001. 3-D Image Processing Algorithms. John Wiley & Sons, Inc, New York.

Reeves, A. P., Kostis, W. J., 2000. Computer-aided diagnosis for lung cancer. Radiologic Clinics of North America 38 (3), 1–11.

TecGraf, G. T. G., 2001. Canvas draw CD. Available at: [http://www.tecgraf.puc-rio.br/cd]. Accessed August 21, 2001.

Tozaki, T., Kawata, Y., Niki, N., Ohmatsu, H., Eguchi, K., Moriyama, N., 1996. Three-dimensional analysis of lung areas using thin slice CT images. In: Hoffman, E. A. (Ed.), Physiology and Function from Multidimensional Images. SPIE : Medical Imaging, Newport Beach, CA, USA, pp. 2–11.

Wood, S. L., Jamali, H., 1992. Segmentation of gray scale sampled images with bimodal source models. In: Conference Record of The Twenty-Sixth Asilomar. Signals, Systems and Computers, pp. 456–460.

Yankelevitz, D. F., Reeves, A. P., Kostis, W. J., Zhao, B., Henschke, C. I., 2000. Small pulmonary nodules : Volumetrically determined growth rates based on CT evaluation. Radiologic Clinics of North America 217, 251–256.